



# ONE-LINE MODEL FOR RIVER MEANDERING EVOLUTION

Kazuhiko MATSUNOBU <sup>1,\*</sup>, Tadaharu ISHIKAWA <sup>2</sup>

<sup>1</sup> *TOKEN C. E. E. Consultants Co., Ltd., 1-15-6, Kita-Otsuka, Toshima Ward, Tokyo 170-0004, Japan;*  
email: [matsunobu-k@tokencon.co.jp](mailto:matsunobu-k@tokencon.co.jp)

<sup>2</sup> *Tokyo Institute of Technology, 4259, Nagatsuta Town, Midori Ward, Yokohama City, Kanagawa Pref. 226-8503, Japan*  
email: [workishikawa0612@yahoo.co.jp](mailto:workishikawa0612@yahoo.co.jp)

**Abstract:** Herein, we report on a one-line model for river meandering evolution that was developed by considering the effects of helical flow. First, flow and riverbed variation in a meandering channel are formulated in one dimension, after which the model is verified by comparing the numerical computation results with the existing flume experimental data. Next, the model for describing channel meandering shape deformation is created geometrically. In this model, the velocity of channel deformations caused by side bank erosion is assumed to be proportional to the linear combination of the intensity of the main stream lateral shift and secondary circulation. The weights of those two factors are determined by a comparison between the model response and empirical rules of meandering wavelengths in actual rivers. Finally, the channel neck cut-off on the channel line deformation area is modeled and the resulting model calculations are compared with meandering wavelength data obtained from Google Earth satellite images.

**Keywords:** River channel meandering, One-dimensional formulation, Secondary flow, Meandering wavelength, Satellite image

---

\* Corresponding author. Email: [matsunobu-k@tokencon.co.jp](mailto:matsunobu-k@tokencon.co.jp)

## 1. Introduction

River meandering on alluvial plains is among the more important research topics in geomorphology and river engineering, as well as the topic of numerous existing case studies and experimental flume studies [1]-[4]. Recently, spurred by advancements in computation technology, a number of horizontal two-dimensional (2D) or three-dimensional (3D) numerical models have been proposed [5]-[8]. Notably, Asahi et al. [5] simulated a channel meandering development process used for modeling side bank erosion and deposition by considering the mechanism outlined in Parker et al. [9]. However, due to various problems such as high computation loads, those researchers were unable to simulate long-term and long-reach meandering channel deformations in 2D or 3D models.

On the other hand, long-time meandering channel deformation processes have been successfully formulated in one-dimensional (1D) equations based on research derived from Ikeda et al. [10]. As an empirical principle, those

equations begin by assuming that the riverbed height difference between the left and right banks is proportional to the curvature of the central river channel axis, as suggested by Engelund [11], and then determine the lateral stream shift of flow velocity. Next, based on another empirical rule [12], they assume that the side bank erosion velocity is proportional to the lateral stream shift. The above process led to the creation of a 1D bend equation that describes the development of a meandering river channel. Since that time, there have been several numerical research efforts that applied those equation results to the bend equation in Ikeda's study [13]-[15].

Noting that stream shifting in meandering river channels is affected by cross-sectional secondary flows caused by the curves of river channel axes, Ishikawa and Kim [16] produced a 1D equation for calculating the main stream shifts and the intensities of the resulting secondary flows. Liu and Ishikawa [17] then improved that 1D model by taking the effect of the stream shift mechanism outlined by Ikeda et al. into consideration using the equation produced by Ishikawa and Kim, after which they applied

the resulting model to laminar flows. From that point, Ishikawa and Liu [18] expanded the theory to cover turbulent flows.

Furthermore, Matsunobu et al. [19] suggested a scheme for calculating the lateral differences of a channel bed by using Ishikawa and Liu's equation without assuming Engelund's empirical rule, which is the base of the model describing the river meandering development process.

In this paper, we report on the construction of a 1D numerical model of river meandering development that works by coupling the computation routine of river meandering development produced via side bank erosion to this meandering channel bed variation model. We then apply our model to actual free meandering rivers and verify its accuracy by comparing the output results with the satellite image data obtained from Google Earth.

## 2. Modeling of meandering flow and channel bed

In this section, we explain the concepts behind the 1D meandering flow model produced by Ishikawa and Liu [18] along with the channel bed variation model outlined in Matsunobu et al. [19]. After that, we explain how we change and combine these models in order to more easily model channel meandering deformation.

The flow model is based on Navier-Stokes equations and a continuity equation in an orthogonal curving coordinate system ( $s, n$ ). As for flow velocity ( $u, v$ ) and water depth  $h$ , we describe the typical distribution profiles seen in the meandering channel flow in five mode functions. Hydraulic quantities, ( $u, v$ ) and  $h$ , are assumed as Eqs. (1) through (3).

$$u = u_0(1 + \beta_1(s)\eta)(\phi(z) + \beta_2\psi(z)) \quad (1)$$

$$v = u_0\{\beta_3(s)\psi(z) + \beta_4(s)(1 - \eta^2)\phi(z)\} \quad (2)$$

$$h = H_0\left\{1 + \beta_5(s)\left(\eta - \frac{1}{3}\eta^3\right)\right\} \quad (3)$$

where  $s, n$ , and  $z$  are longitudinal, transverse, and vertical direction coordinates, respectively, in orthogonal curvilinear coordinate systems,  $u$  and  $v$  are flow velocities in the  $s$  and  $n$  directions, respectively,  $h$  is the water depth,  $\eta$  is a non-dimensional lateral coordinate ( $=2n/B$ ,  $B$ : channel width,  $-1 \leq \eta \leq 1$ ),  $\phi(z)$  is the vertical mode function of the main stream in a straight channel,  $\psi(z)$  is the vertical mode function of secondary circulation flow and uniformization caused by the secondary circulation,  $u_0$  is the cross-sectional average flow velocity, and  $H_0$  is the cross-sectional average water depth.

In Ishikawa and Liu's model,  $h$  is assumed as Eq. (3'). The reason why it is assumed to have a cubic function as shown in Eq. (3) of this study will be discussed later.

$$h = H_0\{1 + \beta_5(s)\eta\} \quad (3')$$

$\beta_1$  to  $\beta_5$  are the variables that represent the intensity of five typical flow patterns in a meandering channel. They depend solely on  $s$ , which is the longitudinal coordinate in a channel. The flow pattern that corresponds to each variable is shown in Table 1. By applying Galerkin integration in a cross section corresponding to the five variables to the basic equations, the model is formulated in one dimension. In other words, the independent variable is exclusively  $s$ .

**Table 1. Variables and correspondent flow pattern**

Variable	Flow pattern
$\beta_1(s)$	Main stream shift
$\beta_2(s)$	Uniformization of main flow
$\beta_3(s)$	Secondary flow
$\beta_4(s)$	Vertically averaged transverse flow
$\beta_5(s)$	Transverse deviation of water depth

Here, the basic equations contain the gradient of  $z$ , as well as the riverbed height in the  $s$  and  $n$  directions. In order to apply the equations to the meandering channels that have the lateral bed slopes, it is necessary to apply some mode function assumptions, such as flow velocity and water depth, to the riverbed topography. In this study, the cross-sectional mode is assumed to be the cubic function, the transverse gradient of which is zero at both sides of the bank, as shown in Eq. (4).

$$z(s, n) = z_0(s) - a(s) \cdot (B/2)(\eta - 1/3\eta^3) \quad (4)$$

where  $a(s)$  is the mode intensity of the cross-sectional riverbed form assumed in this study. The second term on the right-hand side in Eq. (4) is the odd function of eta, which means that if the one side of the bank is eroded, deposits have formed on the other bank. In addition, in order to more easily handle the water surface, the water depth  $h$  is assumed in the cubic function of the same form as Eq. (4), as shown in Eq. (3).

In this riverbed model, the time development of the bed in a meandering channel is computed by combining the riverbed variation to the meandering flow. The 1D bed load model is based on the study by Matsunobu et al. [19]

Eq. (5) is the continuity equation of the bed load.

$$(1 + \sigma n) \frac{\partial z}{\partial t} = - \frac{1}{1 + \lambda} \left( \frac{\partial q_s}{\partial s} + \frac{\partial(1 + \sigma n)q_n}{\partial n} \right) \quad (5)$$

The riverbed is formulated on both sides of the mesh that is divided into two parts in the lateral direction, from which the time development of  $a$ , which is the mode intensity of the riverbed, is computed. The conceptual figure is shown in Fig. 1.

By substituting Eq. (4) into Eq. (5) and integrating the equation in each side in a transverse direction, the bed load balance is described as follows:

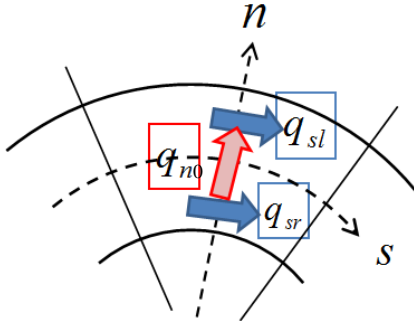


**Fig. 1. Conceptual figure of riverbed computation**

$$\int_{-1}^0 (1 + b\sigma\eta) \left\{ \frac{\partial a}{\partial t} \left( \eta - \frac{1}{3} \eta^3 \right) \right\} d\eta \quad (6)$$

$$= \frac{1}{1 + \lambda} \left( -\frac{\partial q_{sr}}{\partial s} - \frac{\partial q_{n0}}{\partial n} \right)$$

$$\int_0^1 (1 + b\sigma\eta) \left\{ \frac{\partial a}{\partial t} \left( \eta - \frac{1}{3} \eta^3 \right) \right\} d\eta \quad (7)$$

$$= \frac{1}{1 + \lambda} \left( -\frac{\partial q_{sl}}{\partial s} + \frac{\partial q_{n0}}{\partial n} \right)$$

$$q_{sr} = \int_0^1 q_s(s, n) d\eta \quad (8)$$

$$q_{sl} = \int_{-1}^0 q_s(s, n) d\eta \quad (9)$$

$$q_{n0} = q_n(s, 0) \quad (10)$$

By observing the difference between Eq. (6) and Eq. (7), Eq. (11) is obtained and the time development of  $a$  can be calculated.

$$\frac{\partial a}{\partial t} = -\frac{6}{5(1 + \lambda)} \left( \frac{\partial (q_{sl} - q_{sr})}{\partial s} + \frac{q_{n0}}{B} \right) \quad (11)$$

The bed load transport is calculated from the shear stress observed at the riverbed. The functions are suggested by numerous existing studies. In this study, Ashida and Michiue's function [20], as written in Eq. (12), is adopted.

$$q_* = 17\tau_*^{3/2} \left( 1 - \frac{\tau_{*c}}{\tau_*} \right) \left( 1 - \sqrt{\frac{\tau_{*c}}{\tau_*}} \right) \quad (12)$$

where  $q_*$  is a non-dimensional amount of bed load transport,  $\tau_*$  is non-dimensional shear stress, and  $\tau_{*c}$  is non-dimensional critical shear stress.

The shear stress is computed by Eq. (13).

$$\tau_* = \begin{pmatrix} \tau_{*s} \\ \tau_{*n} \end{pmatrix} = \frac{k_f}{R_0 g d} \begin{pmatrix} f u_b \sqrt{u_b^2 + v_b^2} \\ f u_b \sqrt{u_b^2 + v_b^2} \end{pmatrix} + k_g \begin{pmatrix} I_s \\ I_n \end{pmatrix} \quad (13)$$

where  $R_0$  is the relative specific gravity of sediment particles,  $g$  is gravity acceleration,  $d$  is the representative diameter of the sediment particles,  $f$  is the friction coefficient,  $u_b$  and  $v_b$  are (respectively) the flow velocities

**Table 2. Channel configuration in Hasegawa's experiment**

Channel width $B$ [cm]	Longitudinal channel slope $I_{s0}$	Flow discharge $Q$ [L/s]
0.3	0.0141	0.75
Cross-sectional averaged flow velocity $u_0$ [cm/s]	Cross-sectional averaged water depth $H_0$ [cm]	Representative particle diameter $d$ [mm]
32.21	0.89	0.43

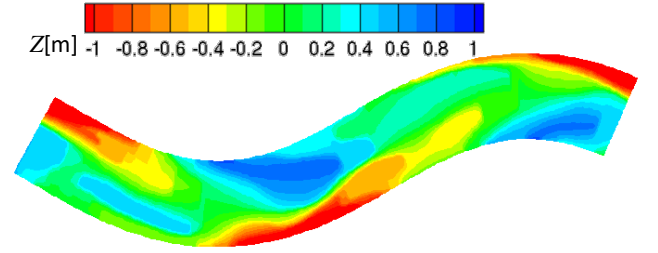


**Fig. 2. Riverbed height in Hasegawa's experiment**

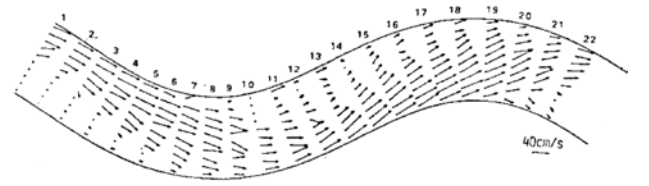


**Fig. 3. Velocity vectors in Hasegawa's experiment**

in the  $s$  and  $n$  directions near the river bed,  $I_s$ , and  $I_n$  are the riverbed slope in the  $s$  and  $n$  directions, respectively ( $=\text{grad } z$ ),  $k_f$  is the rate of effective shear force and all shear forces, and  $k_g$  is the correction coefficient obtained by the shape of the sediment particles.

The first right-hand term in Eq. (13) is the effect of hydrodynamic force achieved by the flow velocity determined by Eqs. (1) and (2), while the second term is the effect of gravity generated by the channel slope determined by Eq. (4).  $k_f$  was determined to be 0.44 via trial computations, and  $k_g$  is 2/3, which is the value obtained when the particles were assumed to be spherical.

The models were then verified with Hasegawa's flume experimental data [21]. Table 2 shows the configuration of the channel, while Figs. 2 and 3 show a contour map of the riverbed height and the flow velocity vectors in the equilibrium state, respectively.

Fig. 4 shows the time development of the amplitude of  $a$ , which is computed under the conditions of Hasegawa's experiment in this model. First, we can see that the channel bed variation rapidly becomes bigger, but the change in time becomes smaller, until an equilibrium state is finally achieved. Fig. 5 compares the longitudinal profile of  $\beta_1$  and

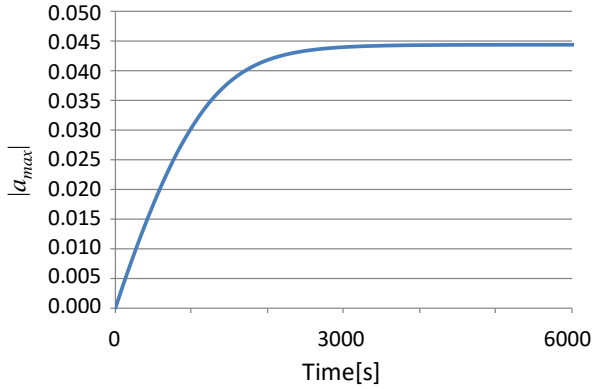


Fig. 4. Time development of the amplitude of  $a$

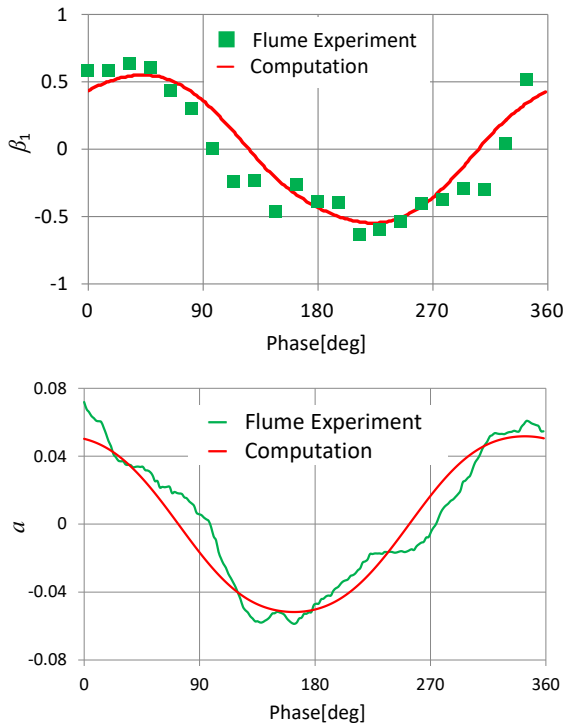


Fig. 5. Longitudinal profile of  $\beta_1$  and  $a$

$a$  between the experimental data and computational results. Here, it can be seen that the computational results roughly agree with those of the flume experiment.

### 3. Modeling of channel deformation by river meandering

In this section, we formulate meandering river channel deformation based on the riverbed variation model constructed in the previous section.

Meandering channel development is determined by the central axis movement of the channel and is the same as the existing 1D model. The deformation velocity is proportional to the intensity of “some pattern of channel flow” in the equilibrium riverbed as seen in Eq. (14).

$$\Delta n = E\Delta t \cdot u_s \quad (14)$$

where  $\Delta n$  is the channel axis movement in the normal direction of the channel,  $\Delta t$  is the time step in the meandering computation,  $E$  is the non-dimensional coefficient of side bank erosion, and  $u_s$  is the flow velocity that controls the velocity of side bank erosion; and is determined by “some pattern of channel flow.”

Here, the existing studies that are derived from Ikeda et al. used  $\beta_1$ , which is the main stream shift intensity.

$$u_s = \beta_1 u_0 \quad (15)$$

The reason for this choice is that the 1D model formulated by Ikeda et al. is based on shallow water equations. Therefore, their model had more limited parameters than the model used in this study. More specifically, they did not use the two parameters, intensity of secondary flow  $\beta_3$  and the uniformization of the main stream, in the vertical direction caused by secondary flow  $\beta_2$ .

On the other hand, in an actual meandering channel, downward and upward flows are generated in the outer and inner bank, respectively. These are caused by the secondary flow that is considered in Ishikawa and Liu’s model. This results from the fact that the outer bank of the channel erodes, while deposits form on the inner bank, as pointed out by Sekine [22].

Therefore, when computing the development of meandering channel form, better results can potentially be obtained by considering the side bank erosion produced by the secondary flow intensity,  $\beta_3$ .

However, the most appropriate method for combining  $\beta_1$  (main stream shift) and  $\beta_3$  (secondary flow intensity) is not yet clear. In this study, we assumed the linear combination as shown in Eq. (16) in order to grasp the general influence trends produced by the change of those two factors.

$$u_s = \{\gamma\beta_1 + (1 - \gamma)\beta_3\}u_0 \quad (16)$$

where  $\gamma$  is an empirical constant for the combination ratio, and when  $\gamma = 1$ , Eq. (16) is equal to Eq. (15).

The movement of the node points  $(x_i, y_i)$  in Cartesian coordinates that is caused by the channel deformation is described in Eq. (17) and is based on  $\Delta n$  obtained by Eq. (14).

$$\begin{aligned} x_i(t + \Delta t) &= x_i(t) - \Delta n \cdot \sin\theta_i \\ y_i(t + \Delta t) &= y_i(t) + \Delta n \cdot \cos\theta_i \\ s_i &= \sum_{i=0}^n \delta s_i = \sum_{i=0}^n \sqrt{\delta x_i^2 + \delta y_i^2} \end{aligned} \quad (17)$$

where  $\theta_i$  is the local angle of the channel from the  $x$  axis,  $(\delta x_i / \delta s_i, \delta y_i / \delta s_i) = (\cos \theta_i, \sin \theta_i)$ ,  $\delta x_i = x_i - x_{i-1}$ ,  $\delta y_i = y_i - y_{i-1}$ ,  $\delta s_i = s_i - s_{i-1}$ , and  $s_i$  is the longitudinal coordinate  $s$  of the  $i$ -th node point.

Each time a new channel form is determined, the mode

intensity parameters in the equilibrium riverbed of the channel condition, including  $\beta_1$  and  $\beta_3$ , are computed. By using them, the new channel form is calculated from Eqs. (14), (16), and (17). Then, by repeating the routine, the time development of river channel meandering can be reproduced.

#### 4. Model verification

Next, we attempted the following numerical experiment aimed at estimating the value of  $\gamma$  in Eq. (18). We began by noting that the wavelength that appears when the meandering deformation of a straight river channel begins is almost the same with that of an alternating bar. In addition, the wavelength  $L$  is roughly proportional to channel width  $B$ , and  $L/B$  is almost equal to 10, as shown in Fig. 6.

Here, the value of  $\gamma$  when the meandering wavelength in the channel meets the condition of  $L/B=10$  under the infinitesimal amplitude is verified with the numerical simulation as described below.

The channel is configured as shown in Table 3, which is the virtual conditions on a scale of actual rivers where the typical free meandering on an alluvial plain can be frequently seen. The initial deformation is given in the form of a long straight channel by a sine-generated curve, as seen in the black line in Fig. 7. The computation results for various values of  $\gamma$  are also shown in the figure. The smaller the values of  $\gamma$  are, more specifically, the bigger the influence of  $\beta_3$  is, the shorter the length of the meandering wave is, and the bigger the amplitude becomes. It can be seen that when gamma is 0.2,  $L/B$  approaches 10.

Next, using satellite images of actual rivers obtained from Google Earth, the central axis lines of 30 meandering sections of rivers around the world, with a variety of river widths, were digitized and the central axes of their meandering waves were estimated. Then, the wavelengths of each of those rivers were computed and compared with the computational results.

As one example, Fig. 8 shows a portion of the upper

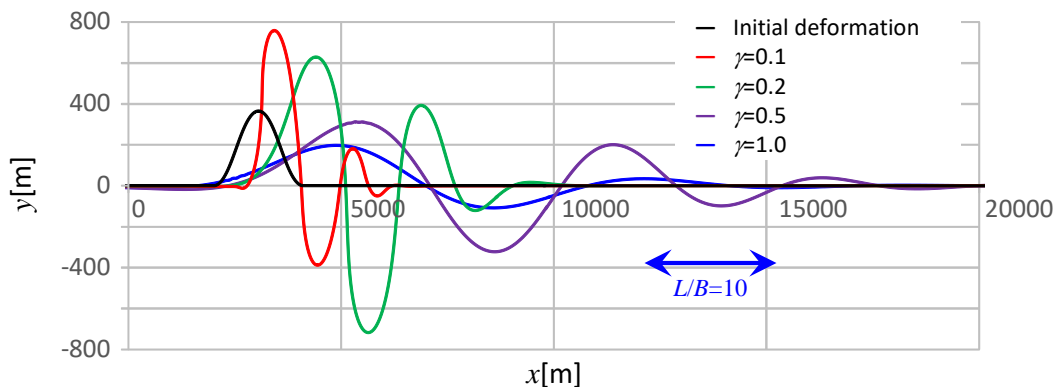


Fig. 7. Development of channel meandering for various values of  $\gamma$

section of the Madeira River, which belongs to the Amazon River system. In this figure, the traced channel line is shown with a red line and the central axis of the meandering is shown with a blue line. Note that the wave half-length is the distance between the two green points that are next to each other.

Fig. 9 is a histogram of  $L/B$ , which is the wavelength

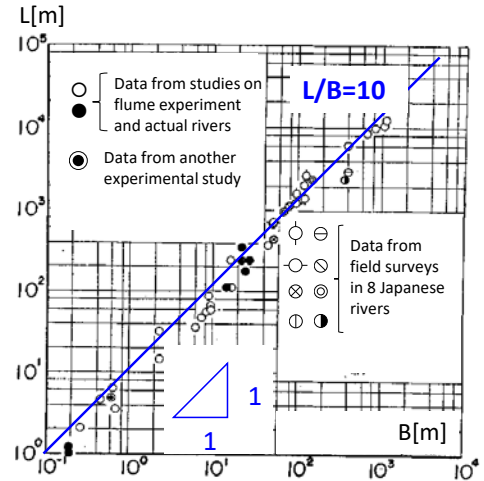
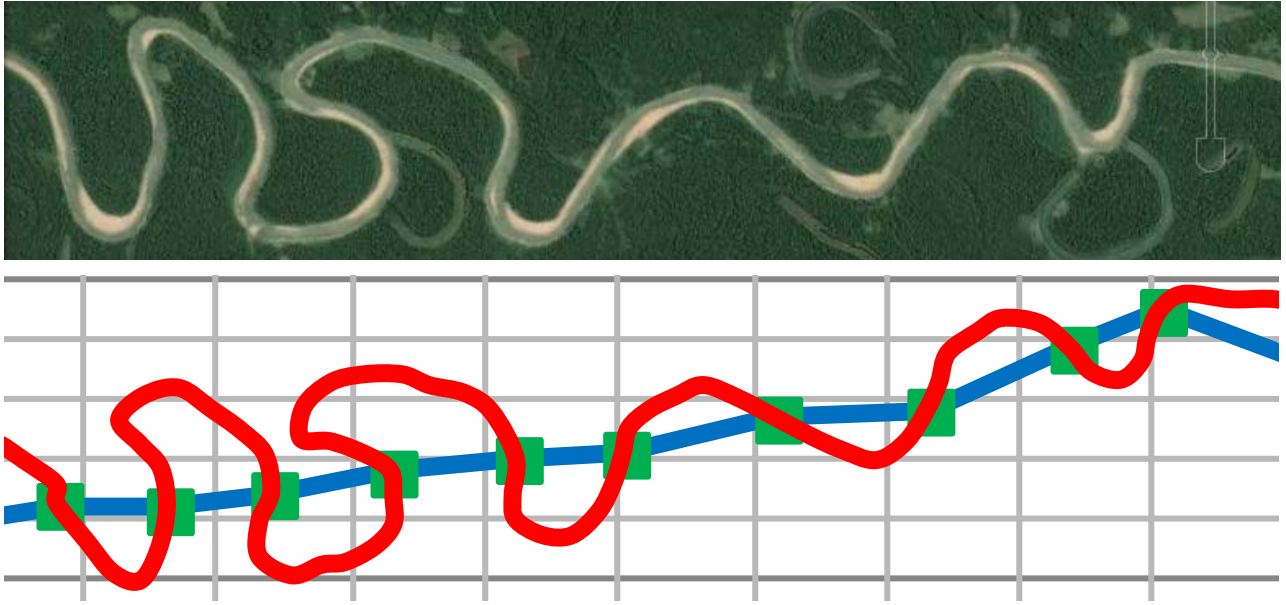


Fig. 6. Relationship between  $L$  and  $B$  in many actual rivers (Committee on hydraulics and hydraulic engineering, JSCE) [23]

Table 3. Channel configuration in the computation of meandering development

Channel width $B$ [m]	Longitudinal channel slope $I_{s0}$	Flow discharge $Q$ [ $\text{m}^3/\text{s}$ ]
300	1/3000	3600
Cross-sectional averaged flow velocity $u_0$ [m/s]	Cross-sectional averaged water depth $H_0$ [m]	Representative particle diameter $d$ [mm]
1.577	7.608	0.768



**Fig. 8. Example of the digitization of satellite images by Google Earth**

in each wave divided by the representative river width. In this figure, the mode value of  $L/B$  is 10, which agrees with the infinitesimal amplitude analysis used in the previous discussion. However, the profile is distorted and the mean value of  $L/B$  is about 19. This suggests that the wavelength becomes bigger as the meandering develops. One possible cause of this is that the number of waves is reduced by the cut-off that results from the increasing amplitude and the approach of side banks in a channel.

The cut-off phenomenon is modeled geometrically as follows: In each step, after the computation of channel deformation, the distance between two nodes ( $i$  and  $j$ : their indices) are computed to produce a judgment, and cut-off occurs if the two nodes meet the conditions of Eqs. (18) and (19).

$$L_{ij} < k_1 B \quad (18)$$

$$S_{ij} < k_2 L_{ij} \quad (19)$$

where  $L_{ij}$  is the straight distance between the two nodes and can result in a cut-off when this value approaches the river width  $B$ . However, if you judge whether channel cut-off occurs only by Eq. (18), it is judged that the cut-off will occur in two nodes which are next to each other. Obviously, that makes no sense either in computations or in actual phenomena. So, to avoid that, the conditions of Eq. (19) are applied.  $S_{ij}$  is the distance along the channel axis between these nodes. By Eq. (19), channel cut-off will occur only when the amplitude of channel meandering becomes large to some extent.

Here,  $k_1$  and  $k_2$  are the coefficients in the value of one or more, and were determined as  $k_1 = 2.0$  and  $k_2 = 3.8$  via trial computations. Finding a more reasonable way to determine these values is a future task. The channels are tied in a cubic Bezier curve that is sequential in angle after the cut-off has occurred. Fig. 10 shows an example of the

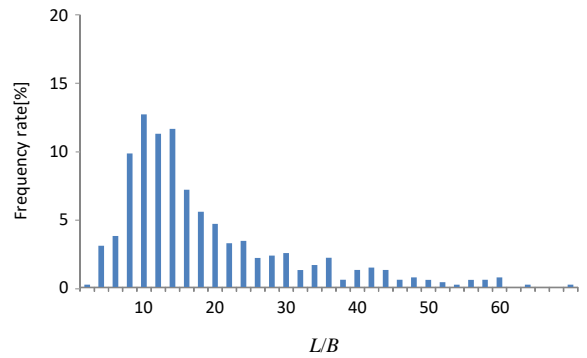


**Fig. 9. Histogram of  $L/B$  in Google Earth images**

channel deformation created by a cut-off.

In eight of the 30 rivers that we analyzed using Google Earth satellite images, we added partial disturbance into the straight channels and then simulated the development and propagation of channel meandering. The red markers in Fig. 11 show the mean wavelength in the computational results of each river, while the green markers show the values obtained by analyzing Google Earth images. Note that the black dots are values extracted from the images of the 22 unexamined rivers, and the blue markers show the computational results obtained via the model set forth in Ikeda et al. That is to say, using Eq. (15) instead of Eq. (16). Here, it can be seen that the computation result of this model agrees more closely with that of the image analysis.

Fig. 12 shows a histogram containing channel information obtained via numerical computations using the same process as seen in Fig. 10. Here, we see that the shape of the Fig. 12 histogram is a little sharper than that seen

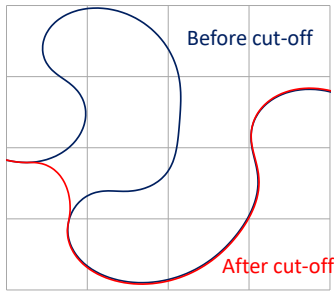


**Fig. 10. Example of channel cut-off**

in Fig. 9. In fact, even though the mode value of  $L/B$  in Fig. 13 is about 11, which nearly matches that seen in Fig. 9, the mean value is 15, which is smaller than the Fig. 9 value. In addition, a second peak can be seen at nearly  $L/B=20$ . One possible reason for these tendencies is that the conditions that exist when channel cut-off occurs are determined in one pair of values,  $k_1$  and  $k_2$  in Eqs. (18) and (19), even though the cut-off phenomenon is essentially a probabilistic event. However, the primary characteristics of the histogram profile, mode, and mean values seen in Fig. 12 are similar to those seen in Fig. 9.

As a specific channel form example, Fig. 13 compares the satellite image and the channel determined by our computational results for a section of the Purus River, which is part of the Amazon River system. Here, we note that qualitatively similar irregularities exist in both channel axes.

There are two mechanisms involved in these irregularities. One relates to the fact that two important parameters ( $\beta_1$  and  $\beta_3$ ), which are used in this study for calculating channel deformation (as shown in Eq. (16)) have different characteristics, including the phase used. The other is the channel cut-off repetition.

## 5. Conclusions

The conclusions of this study are as follows:

1. A 1D meandering flow and riverbed variation model was constructed based on existing models while assuming the lateral riverbed height will be used as a cubic function.
2. This model, which can describe the development of a meandering channel via an examination of side bank erosion, is coupled to the flow and riverbed model. As a new scheme, the velocity of side bank erosion is assumed to depend not only on the main stream shift, but also on the secondary flow intensity.
3. The computations were attempted for the various values of  $\gamma$ , which is the weighted parameter of the linear combination of these two flow patterns. When  $\gamma = 0.2$ , the ratio of the meandering wavelength and

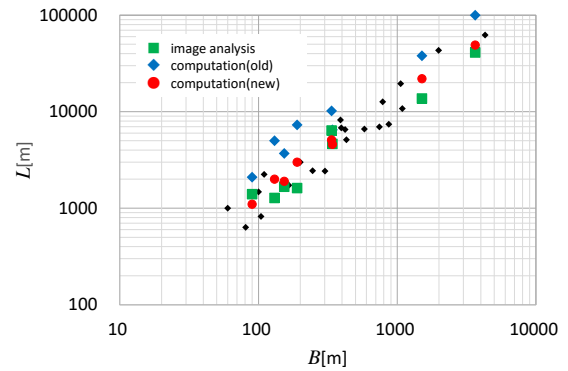


**Fig. 11. Wavelengths comparison**

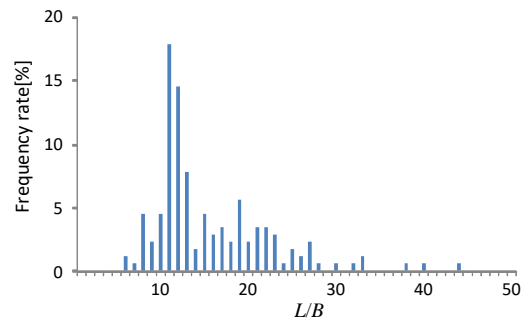


**Fig. 12. Histogram of  $L/B$  in computation results**

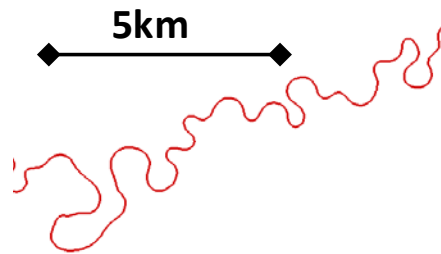


**Fig. 13. Comparison of channel meandering shape**

channel width ( $L/B$ ) obtained from the computations were in good agreement with the observation data.

4. The meandering model was then applied to several actual rivers, after which the channel cut-off mechanism was built into the model. The primary characteristics seen in the histogram of  $L/B$  in computation results agreed well with an analysis of satellite image data obtained from Google Earth. In addition, irregularities in the actual river images can also be seen in the computation results.

## References

1. L.B. Leopold and M.G. Wolman: River Meanders, Geol. Soc. Am. Bull, Vol.71, pp. 769–794, 1960.
2. Hickin, E.J. and Nanson, G.G.: The Character of Channel Migration on the Beaton River, Northeast British Columbia, Canada. Geol. Soc. Am. Bull, Vol.86, pp.487-494, 1975.
3. Friedkin, J.K.: A laboratory study of the meandering of alluvial rivers, U.S. Army Corps of Engineers Waterways Experiment stations, Vicksburg, MS, USA, 1945.
4. Federici B, Seminara.G : On the convective nature of bar instability, Journal of Fluid Mechanics, 487, pp.125-145, 2003.
5. Kazutake Asahi, Yasuyuki Shimizu, Jonathan Nelson, and Gary Parker: Numerical simulation of river meandering with self-evolving banks, J. Geophysical Research, Earth Surface, Vol. 118, pp.2208-2229, 2013.
6. Dong Chen and Jennifer G. Duan: Case study: two-dimensional model simulation of channel migration processes in West Jordan River, Utah, Journal of Hydraulic Engineering, ASCE, Vol.134, No.3, pp.315-327, 2008.
7. Guangqian Wang, Junqiang Xia, and Baosheng Wu: Numerical simulation of lateral channel deformations in the braided reach of the lower yellow river, Journal of Hydraulic Engineering, ASCE, Vol. 134. No.8, pp.1064-1077, 2008.
8. Dongdong Jia, Xuejun Shao: Three-dimensional modeling of bank erosion and morphological changes in the Shishou bend of the middle Yangtze River, Advances in Water Resources, Vol.33, pp. 348-360, 2010.
9. G. Parker, Y. Shimizu, G. V. Wilkerson, E. C. Eke, J. D. Abad, J. W. Lauer, C. Paola, W. E. Dietrich and V. R. Voller: A new framework for modeling the migration of meandering rivers, Earth Surf. Process. Landforms, 36, pp.70-86, 2011.
10. Ikeda, S., Parker, G. and Sawai, K.: Bend theory of river meanders, Part 1. Linear development, Journal of Fluid.Mech., Vol.112, pp.363-377, 1981.
11. Engelund, F.: Flow and bed topography in channel bends, Journal of Hydraulic Division, Proc. ASCE, Vol.100, pp.1631-1648, 1974.
12. Pizzuto,J.E., Meckelnburg,T.S.: Evaluation of a linear bank erosion equation. WaterResour. Res Vol. 25, pp. 1005-1013, 1989.
13. Gary Parker and Edmund D. Andrews: On the time development of meander bends, J. Fluid Mech, Vol. 162, pp. 139-156, 1986.
14. Johannesson, H., and G. Parker: linear theory of river meanders. Pages 181-213 in S.iked and G. Parker (eds.), River meanderings. Water resource monography 12. American geophysical union, Washionton DC., 1989.
15. Sun,T ,Meakin. P.: A simulation model for meandering rivers. Geol. Soc.Amer. Bull. Vol. 110, pp.1485-1498, 1996.
16. T. Ishikawa and S. Kim: A basic study on the development of secondary circulation in curved channels, Journal of JSCE, No.375/II-6, pp.143-149, 1986. (in Japanese)
17. C.Liu and T.Ishikawa: A basic study on the modeling of transverse inequality of flow in meandering river, Journal of JSCE, B1, Vol.68, No.4, pp.1285-1290, 2012.(in Japanese)
18. T.Ishikawa and C.Liu: A basic study on the modeling of lateral stream shift in curved channels, Journal of JSCE, B1, Vol.69, No.1, pp.60-70, 2013. (in Japanese)
19. K.Matsunobu, T.Ishikawa, and M. Ando: 1D modeling of bed deformation in a meandering river, journal of JSCE, B1, Vol.70, No.4, pp.745-750, 2014. (in Japanese)
20. K.Ashida and M.Michiue: Study on hydraulic resistance and bed-load transport rate in alluvial streams, Journal of JSCE, No. 206, pp.59-69, 1972. (in Japanese)
21. K.Hasegawa: A study on flows and bed topographies in meandering channels, Journal of JSCE, No.338, pp.105-114, 1983. (in Japanese)
22. M.Sekine: Study on the channel migration due to a bank erosion, Journal of JSCE, No.533/ II-34, pp.51-59, 1996. (in Japanese)
23. Task committee on the bed configuration and hydraulic resistance of alluvial streams, Committee on hydraulics and hydraulic engineering, JSCE: The bed configuration and roughness of alluvial streams, Journal of JSCE, No.210, pp.85-91, 1973. (in Japanese)